Journal of Applied Physics

Magnetoimpedance and magnetocapacitance of anion-substituted manganese chalcogenides

Cite as: J. Appl. Phys. **121**, 075701 (2017); https://doi.org/10.1063/1.4976097
Submitted: 17 November 2016 . Accepted: 30 January 2017 . Published Online: 15 February 2017

S. S. Aplesnin, O. B. Romanova, V. V. Korolev, M. N. Sitnikov, and K. I. Yanushkevich

Magnetoimpedance and magnetocapacitance of anion-substituted manganese chalcogenides

S. S. Aplesnin,[1,2] O. B. Romanova,[1,a)] V. V. Korolev,[2] M. N. Sitnikov,[2] and K. I. Yanushkevich[3]
[1]*Kirensky Institute of Physics, Federal Research Center KSC SB RAS, Krasnoyarsk 660036, Russia*
[2]*Siberian State Aerospace University M F Reshetnev Corporation, Krasnoyarsk 660014, Russia*
[3]*Scientific-Practical Materials Research Center NAS, Minsk 220072, Belarus*

(Received 17 November 2016; accepted 30 January 2017; published online 15 February 2017)

The magnetoresistive effect in $MnSe_{1-X}Te_X$ manganese chalcogenides with a substitute concentration of $X = 0.1$ is studied by impedance spectroscopy. The magnetoimpedance above the Neel temperature is found. The obtained experimental data are explained in the framework of the model of existence of magnetic nanoareas of two types. Two activation energies in the low- and high-frequency regions are determined from the frequency and temperature dependences of the permittivity described in the Debye model. The extrema found in the temperature dependence of the pyroelectric current are consistent with the maxima in the temperature dependence of magnetization. Temperature dependence of the carrier relaxation time is established. The magnetocapacitance of the $MnSe_{1-X}Te_X$ solid solutions is found. The change in the carrier type above the Neel temperature and the temperature of the transition to the magnetically ordered state in the MnTe nanoarea is established. *Published by AIP Publishing.* [http://dx.doi.org/10.1063/1.4976097]

I. INTRODUCTION

Magnetic semiconductors, which undergo the metal-insulator phase transition and exhibit the magnetoresistive effect, are promising for spintronic and microelectronic applications.[1] The materials that have the magnetocapacitance without magnetoelectric coupling are of great importance for use in technology.[2] It is well known that the Maxwell−Wagner extrinsic effects enhance the permittivity and lead to dielectric relaxation without intrinsic dipolar relaxation.[3] In addition, the Maxwell−Wagner effect can yield the magnetocapacitance without magnetoelectric coupling, when a material exhibits the intrinsic magnetoresistance.[4,5] In principle, one can exploit the magnetocapacitance to construct a magnetic sensor that is sensitive to fields for $H < 10$ kOe within the ideal frequency range of 1 kHz to 1 MHz. Semiconductors with a magnetoresistance without long range magnetic order can find application as materials for making of random access memory. In this case, thermal losses will decrease as a result of the absence of hysteresis in a magnetization curve. The magnetoimpedance may be used as a probe of inhomogeneities.

Recently, there has been a renaissance of interest in radio frequency electrical transport in metallic ferromagnets, following the discovery of a giant magnetoimpedance (GMI) effect in some perovskite manganites $R_{1-X}A_XMnO_3$(Re = trivalent rare–earth ion, A = divalent alkaline–earth ion) in the frequency range f = 0.1–10 MHz.[6,7] This has attracted considerable attention from both the view point of potential applications in novel magnetic sensors and the fundamental physics involved.[8] The observed peak in the ac magnetoresistance close T_C is opposite to the behavior of the grain boundary related magnetoresistance in polycrystalline manganites. Ac magnetoresistance is extremely high compared to a smaller dc magnetoresistance at the same field strength.[9] Since the peak in the ac magnetoresistance close to T_C is suggested to arise from the intragrain contribution, it is also possible that the skin depth is determined by the size of the ferromagnetic metallic grains rather than the size of the samples itself.[10] However, not all ferromagnetic materials, but only those with low resistivity, specific magnetic domain structures with high transverse or circular permeability, and small negative magnetostriction can show the GMI effect.

In contrast to the amorphous ferromagnets and crystalline manganites, we study that antiferromagnetic semiconductors $MnSe_{1-X}Te_X$ show nearly 100% dc magnetoresistance in magnetic field H = 10 kOe.

The MnSe semiconductor compound (starting material) has a NaCl-type face-centered cubic (fcc) structure. In the temperature range of $248\,K < T < 266\,K$, manganese monoselenide undergoes the structural phase transition from the cubic phase to the NiAs-type structure;[11] below these temperatures, the coexistence of two phases is observed.[12] The magnetic structure of the NiAs phase of MnSe is similar to the magnetic structure of MnTe.[13] The temperature of the magnetic phase transition in MnSe in the cubic modification is $T_N = 135\,K$; in the hexagonal NiAs phase, it coincides with the structural transition temperature $T_S = 272\,K$. The magnetoresistive effect was found in the magnetically ordered cubic phase. The magnetoresistance increases upon approaching the Neel temperature and attains 14% in a field of $H = 5$ kOe.[14] In the MnTe film, the magnetoresistive effect is observed at room temperature.[15]

According to the X-ray and neutron diffraction data,[16,17] substitution of tellurium for selenium leads to the suppression

a)Author to whom correspondence should be addressed. Electronic mail: rob@iph.krasn.ru

of the hexagonal phase and to the single-phase state of the $MnSe_{1-X}Te_X$ system with the fcc structure (sp. gr. $Fm\bar{3}m(225)$) in the temperature range of $120\,K < T < 300\,K$. The intensity of peaks in X-ray diffraction patterns decreases, and the intense incoherent X-ray scattering background is formed. Study of the magnetic properties of the $MnSe_{1-X}Te_X$ solid solutions showed a decrease in the paramagnetic Curie temperature and Neel temperature by about 20% with increasing substitute concentration in the anion sublattice. The magnetic moment changes similarly. The anomalous temperature dependences of magnetization and magnetic susceptibility of the $MnSe_{0.9}Te_{0.1}$ solid solutions near a temperature of 330 K are explained by the formation of nanoclusters.[16] For the composition with $X = 0.1$, the negative magnetoresistance in the vicinity of the Neel temperature was found.[18] The decrease in the resistance in the magnetic field is caused by an increase in the electron localization radius in potential wells due to the competition between the ferromagnetic and antiferromagnetic interactions and a decrease in the potential barrier width. It was observed that the spin-glass behavior of the magnetization of the samples cooled with and without magnetic field correlates with the temperature dependence of the magnetoresistance.[19,20]

In the $MnSe_{1-X}Te_X$ solid solutions, nanoareas with different crystal and magnetic structures can form. One of the techniques widely used in studying the electrical properties of inhomogeneous materials is impedance spectroscopy, which allows distinguishing contributions of electric conductivities of different phases, interfaces between the phases, and bulk electric polarization in the material response to an external ac magnetic field and disclosing the microinhomogeneous states.[21–23]

The aim of this study was to establish the carrier transport and scattering mechanisms in anion-substituted semiconductor structures and determine the contributions of nanoareas to the conductivity of the samples using impedance spectroscopy. The other problems to be solved are investigation of the local polarization of the electrically and magnetically inhomogeneous states from the dielectric properties and pyroelectric current and determination of the mobility, sign, and concentration of the majority carriers responsible for the magnetoresistive effect observed in the magnetically ordered region. The observed effects are explained in the framework of the model of coexisting nanoareas with different structures and polymorphous transitions.

II. EXPERIMENTAL

The $MnSe_{1-X}Te_X$ ($X = 0.1$) samples were synthesized by the solid-state reaction in a stepwise mode.[16] The samples had the form of parallelepiped with dimensions approximately $6 \times 4 \times 2\,mm^3$ and were inserted into a cryostat. Silver paste was applied to attach wires to the samples. The electric measurements of the $MnSe_{1-X}Te_X$ ($X = 0.1$) chalcogenide compounds were performed in magnetic fields of up to 13 kOe at temperatures of 80–400 K in the frequency range of $\omega = 0.1$–1000 kHz. The magnetoimpedance measurements were carried out using the analyzer components AM-3028. The magnetic field is parallel to the capacitor plate. The data on the frequency dependence of the impedance are presented in the Nyquist coordinates Z'-iZ'', where Z' is the real component (active impedance) and Z'' is the imaginary component (reactive impedance). The complex permittivity of $MnSe_{1-X}Te_X$ was determined on the basis of the capacitance measured by an AM-3028 LCR Meter at the frequencies of 0.1–1000 kHz without field and in a magnetic field of 13 kOe in the temperature range of 80–500 K. The Hall coefficient was measured on rectangular samples by a four-probe technique in the dc mode at temperatures of 100–400 K in magnetic fields of up to 12 kOe. When measuring the Hall coefficient, we took into account the contributions of the spurious emf caused by galvanomagnetic and thermomagnetic side effects and the asymmetry of contacts (zero field measurements). The pyroelectric current was measured with a Keithley 6517b electrometer in a cryostat at a temperature stabilization accuracy of 0.01 K. The sample was placed between the capacitor plates with a layer of mica to prevent leakage currents.

III. EPERIMENTAL RESULTS AND DISCUSSION

In certain cases, impedance spectroscopy makes it possible to distinguish and determine the contributions of different elements of the microstructure to the total conductivity of a polycrystalline sample. In the framework of the Maxwell–Wagner model,[23] the $MnSe_{1-X}Te_X$ sample under study is considered to be a part of the homogeneous medium containing nanoareas formed by selenium ions $MnSe^{HS}$ with the hexagonal structure and MnTe with the cubic structure (Fig. 1(a)).

The contact potential difference induces a local electric field around these areas, which is compensated in part by impurity carriers. Upon heating to 200 K, the magnetic order in the $MnSe^{HS}$ nanoarea vanishes and the absolute value of

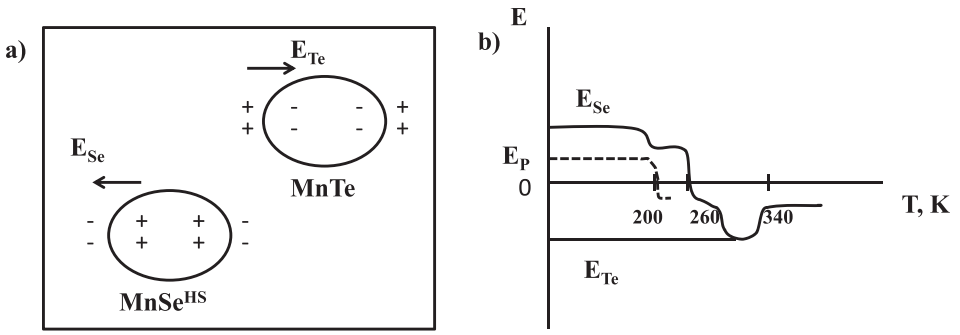

FIG. 1. Uniform medium including hexagonal $MnSe^{HS}$ and cubic MnTe nanodomains in the $MnSe_{0.9}Te_{0.1}$ sample (a). Electrical field created by $MnSe^{HS}$ and cubic MnTe nanodomain versus temperature (b).

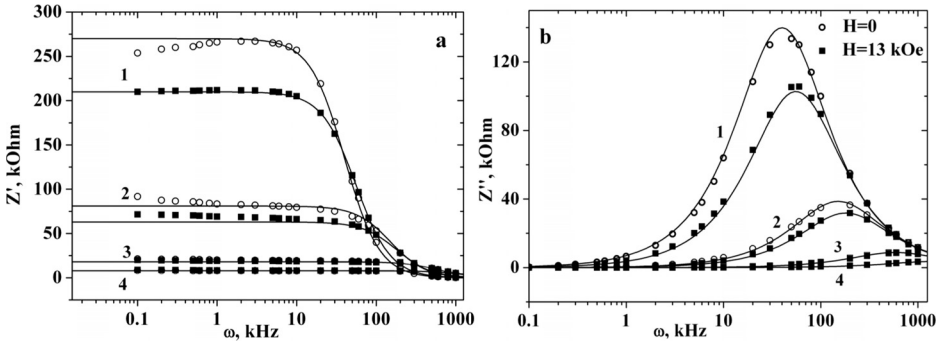

FIG. 2. The frequency dependencies of the real (a) and imaginary (b) part of impedance for the sample $MnSe_{0.9}Te_{0.1}$ measured in the zero magnetic field and in the field 13 kOe at T = 80 K(1), 140 K (2), 200 K (3), and 250 K (4). Experimental results are described in terms of the Debye model (solid line).

the effective potential decreases by the value of the spin-polaron interaction $I_{sd}\ s\langle S^z\rangle/2$, where I_{sd} is the exchange interaction between spins of the localized and band electrons, s is the electron spin, and $\langle S^z\rangle$ is the $MnSe^{HS}$ magnetic moment. At a temperature of 260 K, the nanoareas with the hexagonal phase disappear, which leads to the change in the polarization sign (Fig. 1(b)). Disappearance of the magnetic order in MnTe at 340 K causes a decrease in the effective potential, local polarization, and magnetization of the $MnSe_{1-X}Te_X$ solid solution.

We establish the formation of nanoareas with different magnetic and electrical properties from the frequency dependences of the real (Fig. 2(a)) and imaginary (Fig. 2(b)) parts of the impedance measured in the temperature range of 80–320 K without field and in a magnetic field of 13 kOe. We distinguish two frequency regions in the $Z'(f)$ dependence. In the low-frequency region, the real part of the impedance decreases with increasing temperature. In the frequency region from 50 kHz to 1000 kHz, the frequency dependence of Z' is approximated well by the Mott-type power function $Z'(f) = B/\omega^2$ in the magnetically ordered region.[24] In this frequency region, the key role is played by the transitions of electrons to the near centers and the main contribution to the conductivity is made by the electronic transitions with the intercenter distances of about optimal hopping length. In the low-frequency region, the real part of the impedance is much larger than the imaginary part. The maximum variation in the real part of the impedance is observed at temperatures of the magnetic transition in the low-frequency range, which is larger than the imaginary part of the impedance by an order of magnitude. The Z'' value grows with frequency and passes through its maximum at $\omega = 10-1000$ kHz. As the frequency is further increased, the imaginary part of the impedance decreases. In addition, the values of both real and imaginary components of the impedance decrease under external magnetic field. A similar situation is observed for the manganite.[25]

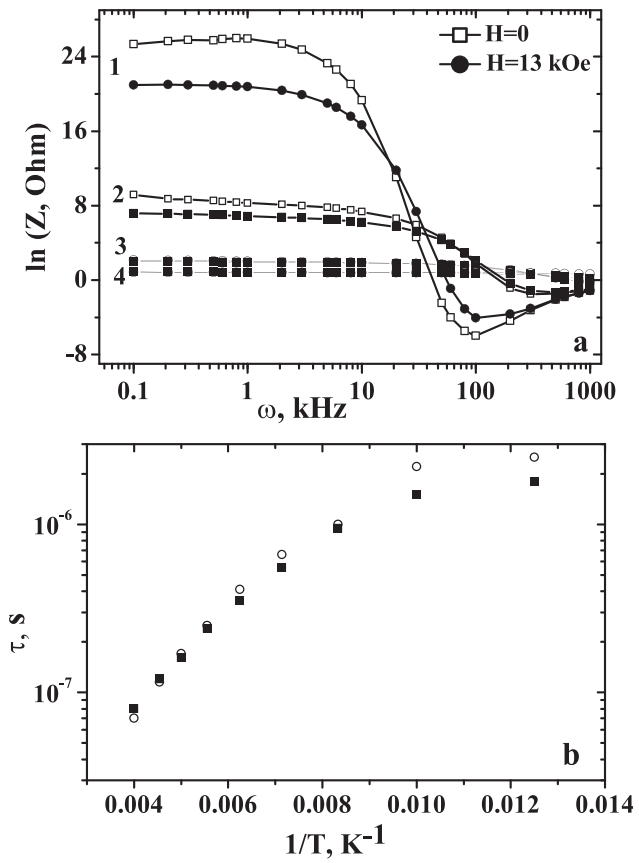

FIG. 3. The frequency dependencies of the impedance (a) that is measured in the zero magnetic field and in the field 13 kOe at temperatures 80 K (1), 140 K (2), 200 K (3), and 250 K (4). The temperature dependence of the relaxation time (b) that is measured in the zero magnetic field and in the field 13 kOe for the $MnSe_{0.99}Te_{0.1}$ sample.

Figure 3(a) shows the frequency dependence of the impedance in magnetic fields of $H = 0$ and $H = 13$ kOe at temperatures of 80–320 K. The total impedance decreases with increasing temperature and magnetic field. The frequency dependences of the imaginary and real parts of the impedance (Figs. 2(a) and 2(b)) are described well by the Debye model at $\omega > 1$ kHz:

$$\mathrm{Re}\,Z(\omega) = \frac{A}{1+(\omega\tau)^2}; \quad \mathrm{Im}\,Z(\omega) = \frac{B\omega\tau}{1+(\omega\tau)^2}. \qquad (1)$$

Here, parameters A and B are constant and temperature-independent and τ is the relaxation time. Fig. 3(b) shows the relaxation time, which monotonically decreases with increasing temperature and depends on the magnetic field. The temperature dependence of the carrier relaxation time obeys the exponential law $\tau = \tau_0 \exp(\Delta E/T)$. The activation energy above the Neel temperature was found to be $\Delta E = 251\ \mathrm{cm}^{-1}$ in the zero magnetic field and $207\ \mathrm{cm}^{-1}$ in a field of 13 kOe. In the magnetically ordered region, the activation energy decreases by more than order of magnitude, $\Delta E = 8\ \mathrm{cm}^{-1}$. The carrier relaxation is caused by the interaction of electrons with the acoustic and optical oscillation modes, which leads to the occurrence of a new oscillation mode. The

combination of the optical and acoustic phonon modes TO+LA(X) was observed in Raman spectra of MnSe at a frequency of 251 cm^{-1}.[26] In the magnetically ordered phase, the carrier energy loss is caused by carrier scattering on spin excitations by the exchange coupling. In addition, the Raman spectra of MnSe revealed a single-magnon excitation with the energy of 18 cm^{-1}.

The impedance spectra (hodograph curves) of the $MnSe_{1-X}Te_X$ sample with a substitute concentration of $X = 0.1$ are presented in Figs. 4(a)–4(c). Dots show the experimental data and solid lines, the results of the graphic-analytical calculation. The experimental data were analyzed using the approximation of equivalent circuits, which include the low- (R_L, C_L) and high-frequency (R_H, C_H) RC chains. The contribution of the bulk part of the Mn−Se−Te system with the cubic structure to the conductivity (denoted as RC in the circuit) is taken into account. This contribution is observed in the form of tails in the impedance spectra over the entire measuring temperature range at frequencies below 1 kHz. The hodograph shown in Fig. 4(a) at $T = 320$ K is described by one circumference corresponding to the R_LC_L chain. As can be seen in Fig. 1, in this temperature region the contribution of MnTe nanoareas prevails. At the rest temperatures in the range from 80 to 250 K, the impedance hodograph contains two pronounced semicircumference regions of the $MnSe^{HS}$ and MnTe nanoareas, which correspond to the low- (R_L, C_L) and high-frequency (R_H, C_H) regions, respectively. At a temperature of $T = 80$ K, the impedance hodograph is described by a semicircumference with the impedance exceeding the impedance measured in the magnetic field by 30%. The maximum impedance variation in the magnetic field $\delta(Z) = \frac{(Z(H)-Z(0))}{Z(0)} \cdot 100\%$ attains 35% at $T = 100$ K; upon further heating, the magnetoimpedance decreases to 2% at T = 250 K in the frequency range from 10 kHz to 1000 kHz (Fig. 5). In the low-frequency range, the magnetoimpedance attains its maximum values of 54% and 20% at temperatures of $T = 120$ and 180 K in the frequency range of 1 kHz–50 kHz. In the vicinity of the Neel temperature, the impedance is independent of magnetic field. Possibly, the active resistance decreases in magnetic field and reactive resistance sharply increases for $MnSe^{HS}$. In the result, the sign of impedance in the magnetic field may be changed for $MnSe^{HS}$ as compared to the MnTe nanoarea where the magnetoimpedance reveals the opposite sign.

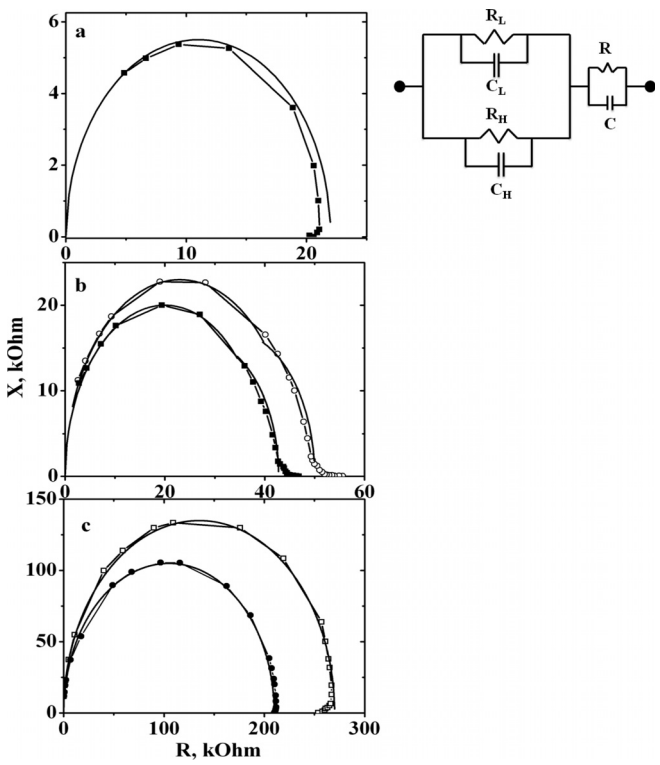

FIG. 4. The impedance hodographs that is measured at the zero magnetic field and in the field 13 kOe at T = 320 (a), 160 K (b), and 80 K (c). The impedance hodographs for equivalent circuit (lines) that is shown in the inset, where R_H, C_H—resistance and capacitance of cubic MnTe nanodomains, R_L, C_L—resistance and capacitance hexagonal $MnSe^{HS}$, and R, C—the resistance and capacitance of the uniform part of the sample Mn-Se-Te.

The frequency dependence of the permittivity measured in the temperature range of 80–250 K with a pitch of 20 K is presented in Figs. 6(a) and 6(b). We present the permittivity as a sum of the permittivities of the $MnSe^{HS}$ and MnTe nanoareas. In the low–frequency region, the contribution of manganese selenide with the hexagonal structure decreases with increasing temperature and above 250 K the inflection in the $Re(\varepsilon(\omega))$ dependence vanishes.

The frequency dependence of the real part of the permittivity is described well in the Debye model with two relaxation times for the $MnSe^{HS}$ and MnTe nanoareas. As the temperature is increased, the permittivity increases with the frequency at $\omega < 1$ kHz.

This is possibly related to diffusion of charged defects in the lattice. The dielectric loss shown in Fig. 6(b) is caused by conductivity σ and described well by the dependence $Im(\varepsilon) = \frac{\sigma}{\varepsilon_{0\omega}}$. The Debye contribution exists, but it is very small. In the magnetic field, the permittivity increases and the magnetocapacitance $\delta\varepsilon = \frac{(\varepsilon(H)-\varepsilon(0))}{\varepsilon(0)}$ attains 5%–6%. The temperature behavior of magnetocapacitance is analogous to that of the magnetoimpedance in the low-frequency region with minimum $\delta\varepsilon$ at $T = 140$ K and maximum $\delta\varepsilon$ at 180 K.

Figs. 7(a) and 7(b) show the temperature dependences of the real and imaginary parts of the permittivity, which

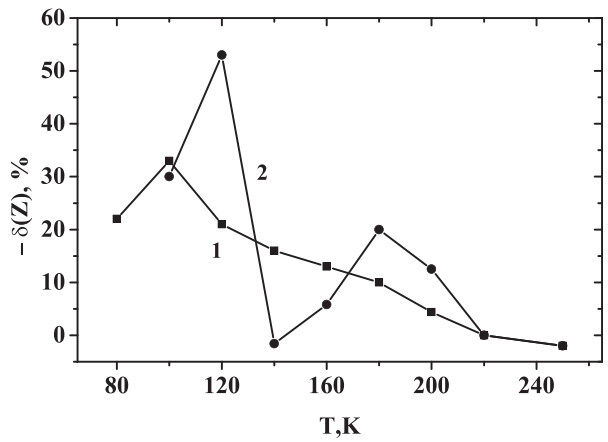

FIG. 5. Temperature dependence of the relative change in the impedance $\delta(Z) = \frac{(Z(H)-Z(0))}{Z(0)} \cdot 100\%$ in the high-frequency range (1) and the low-frequency range (2) for $MnSe_{0.9}Te_{0.1}$.

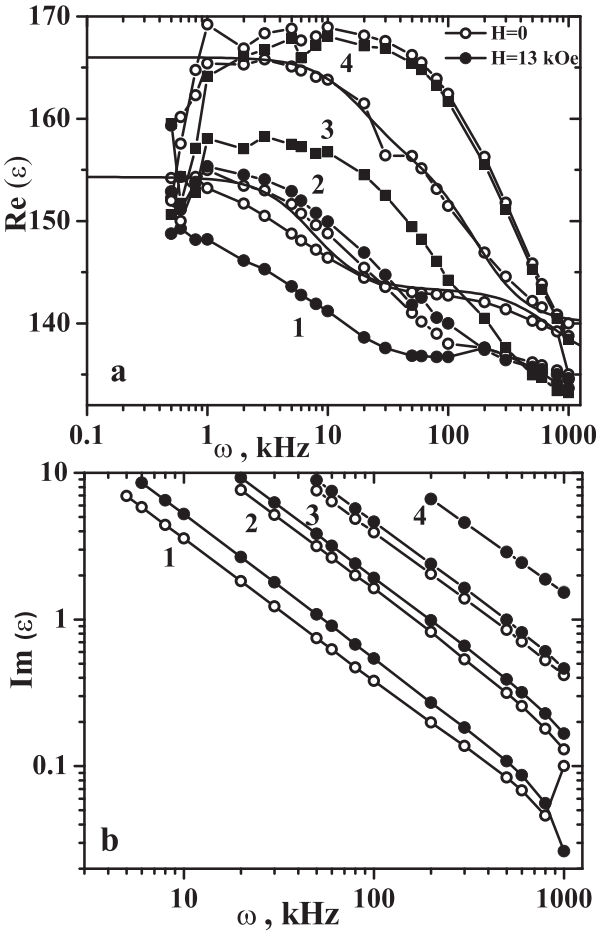

FIG. 6. The frequency dependence of the real (a) and imaginary (b) parts of permittivity of manganese chalcogenide $MnSe_{0.9}Te_{0.1}$ at temperatures 80 K (1), 140 K (2), 180 K (3), and 250 K (4). Solid lines—the fitted function calculated in terms of the Debye model (2–4).

were measured in the frequency range of 1 kHz–300 kHz. The permittivity has a small maximum at $T = 107$ K, the temperature of which is frequency-independent. This is possibly due to the deformation of the crystal structure at this temperature. The temperature dependence is satisfactorily described within the Debye model for the two nanoareas $\varepsilon = \varepsilon_L + \varepsilon_H$:

$$\begin{aligned} Re\,\varepsilon_L(\omega) &= \frac{A}{\left(1+(\omega\tau_L)^2\right)} + \varepsilon_{0L}; \\ Im\,\varepsilon_L(\omega) &= \frac{A\omega\tau_L}{\left(1+(\omega\tau_L)^2\right)} + \frac{\sigma}{\varepsilon_0\omega}, \quad (\mathrm{MnSe^{HS}}), \end{aligned} \tag{2}$$

$$Re\,\varepsilon_H(\omega) = \frac{C}{\left(1+(\omega\tau_{H1})^2\right)} + \frac{D}{\left(1+(\omega\tau_{H2})^2\right)} + \varepsilon_{0H}, \tag{3}$$

$$Im\,\varepsilon_H(\omega) = \frac{C\omega\tau_{H1}}{\left(1+(\omega\tau_{H1})^2\right)} + \frac{D\omega\tau_{H2}}{\left(1+(\omega\tau_{H2})^2\right)} + \frac{\sigma}{\varepsilon_0\omega},$$
$$\omega \geq 10\mathrm{kHz}\ \ (\mathrm{MnTe}). \tag{4}$$

Here, A, C, and D are constants; and τ_L and $\tau_{H1,2}$ are the respective relaxation times for manganese selenide with the

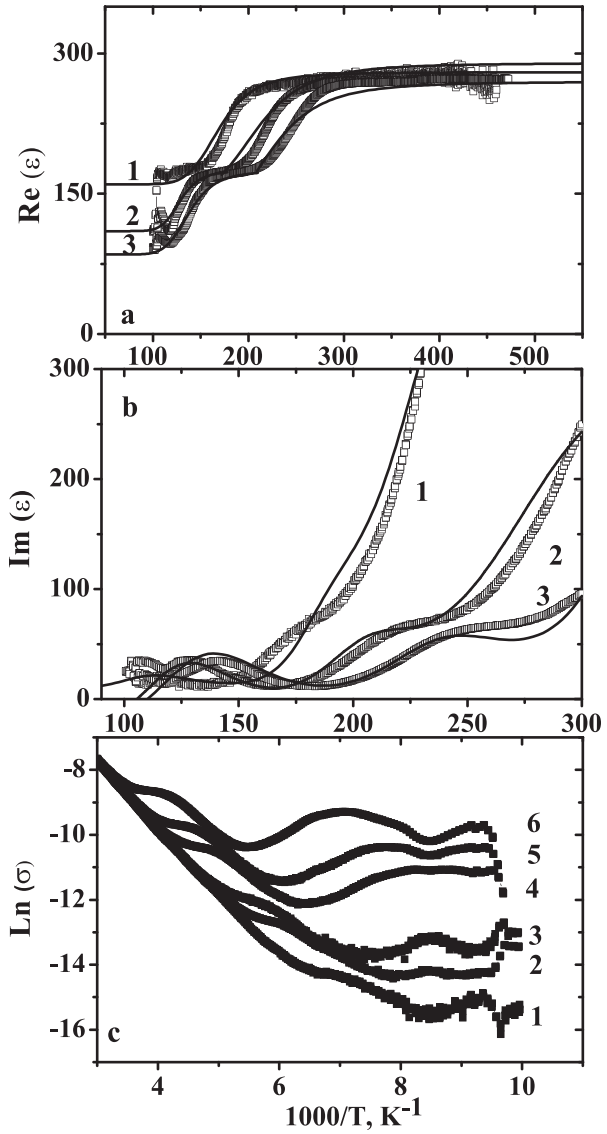

FIG. 7. Temperature dependence of the real (a) and imaginary parts (b) of the permittivity for manganese chalcogenide $MnSe_{0.9}Te_{0.1}$ at frequencies 10 kHz (1), 100 kHz (2), and 300 kHz (3). Solid lines—the fitted function for real (a) and imaginary parts (b) of the permittivity calculated in terms of the Debye model (2–4). The temperature dependence of the conductivity (c) of the sample $MnSe_{0.9}Te_{0.1}$ at frequencies 1 kHz (1), 5 kHz(2), 10 kHz(3), 50 kHz(4), 100 kHz(5), and 300 kHz(6).

hexagonal lattice and manganese telluride, which follow the Arrhenius law, with the activation energies of $\Delta E_L = 0.13$ eV, $\Delta E_{H1} = 0.069$ eV, and $\Delta E_{H2} = 0.17$ eV. The dielectric loss Im(ε) increases upon heating, depends on frequency, and originates from the sample conductivity (Fig. 7(b)). At temperatures above 250 K, the dispersion in the conductivity $\sigma = \mathrm{Im}(\varepsilon)\varepsilon_0\omega$ is missing and the activation energy (ΔE) lies between 0.35 and 0.39 eV (Fig. 7(c)). The activation energy of the ac conductivity exceeds that of the dc conductivity $\Delta E \approx (0.07–0.09)$ eV.[18] The dc conductivity of the $MnSe_{1-X}Te_X$ solid solution is implemented by charged structural defects and the ac conductivity, by carriers in the polarized $MnSe^{HS}$ and MnTe nanoareas. The contribution of band electrons to the permittivity (plasmon contribution) n_e/ω^2 is small, since the capacitance is temperature-independent at T > 200 K and frequency-independent.

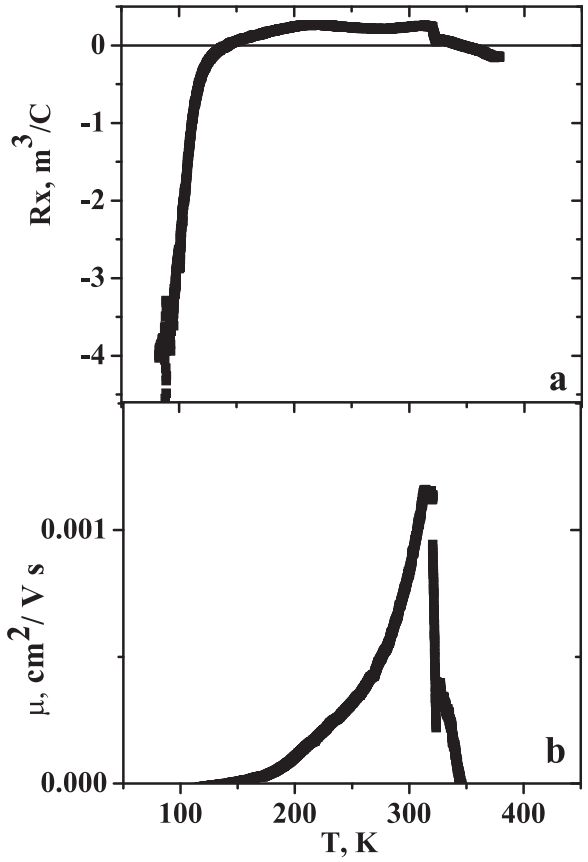

FIG. 8. The temperature dependence of the Hall coefficient (a) and the mobility of the charge carriers (b) for sample $MnSe_{0.99}Te_{0.1}$.

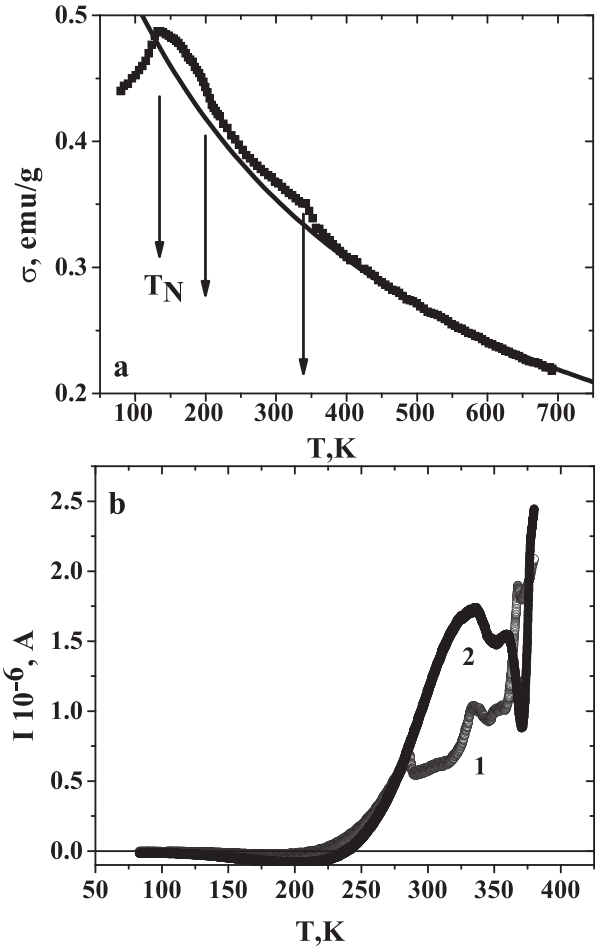

FIG. 9. The temperature dependence of the magnetization measured in a magnetic field 8.6 kOe (a) and pyroelectric current (b) measured in zero magnetic field (1) and H = 13 kOe (2). Arrows indicate the temperature anomalies (T_N = 132 K, 200 K, and 340 K). Magnetization determined from the Cure–Weiss function $\sigma = C\ H/(T+\Theta)$, where C—Cure–Weiss constant, $\Theta = -350$ K (solid line).

Figs. 8(a) and 8(b) show temperature dependences of the Hall coefficient and carrier mobility, which were measured in a magnetic field of 12 kOe at temperatures of 77–400 K. Manganese selenide MnSe has the p-type conductivity. Substitution of tellurium for selenium leads to the change in the carrier sign. As the temperature is increased, the Hall coefficient (R_H) grows; at 140 K, the Hall coefficient changes its sign and the magnetoresistive effect in the $MnSe_{1-X}Te_X$ ($X = 0.1$) attains its maximum.[19] In the temperature range of 140–347 K, the hole conductivity prevails and the Hall coefficient sharply drops at $T = 320$ K. In manganese chalcogenides $MnSe_{0.9}Te_{0.1}$, the Hall mobility has its maximum value of 0.001149 cm^2/V s at $T = 313$ K.

The positions of the energy levels of the $MnSe^{HS}$ and MnTe nanoareas with respect to the chemical potential were determined from the pyroelectric current (Fig. 9(b)). Manganese selenide with the hexagonal structure has the positive potential. Above 200 K, the $MnSe^{HS}$ subband narrows with the vanishing of the magnetic order at this temperature (Fig. 1(b)). This leads to the potential shift in the $MnSe^{HS}$ nanoarea and inversion of the sign of internal electric field induced by the MnTe nanoarea. The temperatures $T = 200$ K and 340 K at which the magnetization sharply increases (Fig. 9(a)) are consistent with the extremum in the temperature dependence of the pyroelectric current (Fig. 9(b)). Below 217 K, the pyroelectric current acquires negative values and is minimum at $T = 190$ K. In the magnetic field, the pyroelectric current changes its sign at $T = 240$ K and attains minimum at T = 200 K. The pyroelectric current maximum is observed at $T = 336$ K and also increases by a factor of 2 in the magnetic field at 290–360 K. The sharp growth of the pyroelectric current above 330 K is caused by a decrease in the polarization MnTe nanoarea (Fig. 1(b)).

Upon approaching the magnetic transition temperature, the anisotropy field decreases and the magnetic moments of nanoareas turn in the external magnetic field direction, which is accompanied by an increase in the magnetic induction $B = \mu_0(H + 4\pi M)$. The mobility and concentration of carriers, whose velocity is orthogonal to the direction of magnetic induction, increase and the pyroelectric current grows. The difference in the carrier sign between the Hall and pyroelectric current data is caused by the value of the current, since the current in the Hall voltage measurements exceeds the pyroelectric current by three orders of magnitude.

IV. CONCLUSIONS

Two regions, low and high frequency, with different impedance and permittivity behaviors were established in the frequency range of 0.1–1000 kHz. The frequency dependences of the real and imaginary parts of the total

impedance are described using the Debye model, which yielded the relaxation time, whose temperature dependence obeys the Arrhenius law with two activation energies above and below the Neel temperature. In the paramagnetic region, the activation energy is related to the interaction of carriers with the combined acoustic and optical oscillation mode. It was found that the activation energy decreases in the magnetic field. It was demonstrated that the impedance decreases in the magnetic field and the magnetoimpedance vanishes above 250 K.

The frequency dependence of the permittivity is described within the Debye model with two activation energies. It was found that the permittivity increases in the magnetic field. In the temperature range of 250–450 K, the permittivity is temperature-independent and the dielectric loss is caused by carriers.

The Hall measurements revealed the change in the majority carrier type upon temperature variation. In the magnetically ordered and high-temperature regions, the majority carriers are electrons and, above the Neel temperature, holes. The magnetic-field dependence of the pyroelectric current and the inversion of its sign upon temperature variation were determined.

ACKNOWLEDGMENTS

The reported study was funded by the Russian Foundation for Basic Research, Government of Krasnoyarsk Territory, Krasnoyarsk Region Science and Technology Support Fund to the research project No. 17-42-240079 r_sibir_a. This study was supported by the Russian Foundation for Basic Research project No. 16-52-00045 Bel_a and government work No. 114090470016.

[1]S. A. Wolf, D. D. Awschalom, R. A. Buhrman, J. M. Daughton, S. von Molnár, M. L. Roukes, A. Y. Chtchelkanova, and D. M. Treger, Science **294**, 1488 (2001).
[2]W. Eerenstein, N. D. Mathur, and J. F. Scott, Nature **442**, 759 (2006).
[3]J. C. Maxwell, *Treatise on Electricity and Magnetism* (Dover, New York, 1991), Vol. 2, pp. 1831–1879.
[4]G. Catalan, Appl. Phys. Lett. **88**, 102902 (2006).
[5]M. M. Parish and P. B. Littlewood, Phys. Rev. Lett. **101**, 16602 (2008).
[6]S. E. Lofland, S. M. Bhagat, S. D. Tyagi, Y. M. Mukovskii, S. G. Karabashev, and A. M. Balbashov, J. Appl. Phys. **80**, 3592 (1996).
[7]P. V. Patanjiali, P. Theule, N. Hakim, S. Sridhar, R. Suryanarayanan, M. Apostu, G. Dhalenne, and A. Revcolevschi, Phys. Rev. B **60**, 9268 (1999).
[8]L. V. Panina, K. Mohri, T. Uchiyama, M. Noda, and K. Bushida, IEEE Trans. Magn. **31**, 1249 (1995).
[9]A. Rebello and R. Mahendiran, EPL **86**, 27004 (2009).
[10]A. Rebello, V. B. Naik, and R. Mahendiran, J. Appl. Phys. **106**, 073905 (2009).
[11]D. L. Decker and R. L. Wild, Phys. Rev. B **4**, 3425 (1971).
[12]J. B. C. Efrem D'Sa, P. A. Bhobe, K. R. Priolkar, A. Das, P. S. R. Krishna, P. R. Sarode, and R. B. Prabhu, Pramana J. Phys. **63**, 227 (2004).
[13]J. B. C. Efrem D'Sa, P. A. Bhobe, K. R. Priolkar, A. Das, S. K. Paranjpe, R. B. Prabhu, and P. R. Sarode, J. Magn. Magn. Mater. **285**, 267 (2005).
[14]S. S. Aplesnin, L. I. Ryabinkina, O. B. Romanova, D. A. Balaev, O. F. Demidenko, K. I. Yanushkevich, and N. S. Miroshnichenko, Phys. Solid State **49**, 2080 (2007).
[15]D. Kriegner, K. Výborný, K. Olejník, H. Reichlová, V. Novák, X. Marti, J. Gazquez, V. Saidl, P. Nêmec, V. V. Volobuev, G. Springholz, V. Holý, and T. Jungwirth, Nat. Commun. **7**, 11623 (2016).
[16]S. S. Aplesnin, O. B. Romanova, M. V. Gorev, A. D. Vasil'ev, O. F. Demidenko, G. I. Makovetskii, and K. I. Yanushkevich, Phys. Solid State **54**, 1374 (2012).
[17]K. E. Engle, J. B. C. Efrem D'Sa, A. Das, and K. R. Priokar, J. Magn. Magn. Mater. **347**, 68 (2013).
[18]S. S. Aplesnin, O. B. Romanova, and K. I. Yanushkevich, Phys. Status Solidi B **252**, 1792 (2015).
[19]O. B. Romanova, S. S. Aplesnin, A. M. Vorotynov, G. I. Makovetskii, O. F. Demidenko, and K. I. Yanushkevich, Solid State Phenom. **233–234**, 447 (2015).
[20]L. Jindong, C. Xiaomin, T. Fei, and M. Xiangshui, J. Appl. Phys. **116**, 043901 (2014).
[21]G. W. Charache and E. W. Maby, J. Appl. Phys. **78**, 3488 (1995).
[22]V. V. Brus, Semicond. Sci. Technol. **28**, 025013 (2013).
[23]E. Barsoukov and J. R. Macdonald, *Impedance Spectroscopy. Theory, Experiment and Applications* (John Wiley & Sons, Inc., Publication, 2005), p. 606.
[24]N. F. Mott, Philos. Mag. **22**, 7 (1970).
[25]C. M. Fu, K. S. Hsu, M. L. Lin, and Z. H. Wen, J. Magn. Magn. Mater. **209**, 151 (2000).
[26]A. Milutinovoć, Z. V. Popović, N. Tomić, and S. Dević, Mater. Sci. Forum. **453–454**, 299 (2004).